A 2D Process-based Morphodynamic Model for Flooding by Non-cohesive Dyke Breach

Mingfu Guan[1]; Nigel G. Wright[2]; P. Andrew Sleigh[3]

Abstract: Inundation models based on the Shallow Water Equations (SWE) have been shown to perform well for a wide variety of situations even at the limit of their theoretical applicability and, arguably, somewhat beyond. One of these situations is the catastrophic event of floods induced by dyke breach and consequent dyke erosion. The dyke collapse is often not sudden - as assumed by many flood simulations in which the dyke boundary is treated as a "dam-break". The dyke erosion is a gradual and complex process that delays the onset of the flood, affecting the hydrograph of the flow. To simulate correct temporal passage of a flood, it is important to understand the rate at which these dykes collapse. In this paper an overtopping flood event combined with dyke erosion is simulated. The model is built upon the 2D Shallow Water Equations together with sediment-flow interactions and incorporates a sediment transport equation. The model is solved using a second-order Godunov-type finite volume method that is accurate and robust. For breach formation, the lateral erosion collapse due to slope instabilities has a significant impact and must be considered, in this paper a simple mathematical approach in two dimensions is proposed to evaluate the stability of lateral bed slope. Several experimental tests are used for validating the morphodynamic model. It is verified that the simulated results agree well with measured data, and that the model predicts such flow phenomena effectively. The validated model is applied to predict a flood event caused by dyke breach with an initial trapezoidal shape due to flow overtopping. The predicted results for the flood event indicate that the 2D process-based morphodynamic model is capable of simulating the spatial and temporal changes of the flood event, including predicting the outflow hydrograph with good agreement, as well as the erosion of the dyke and subsequent deposition process.

Keywords: dyke breach; flow overtopping; morphodynamic model; sediment transport

Introduction

Inundation modeling is significant in flood risk management and disaster prevention and mitigation. A key example of inundation, the catastrophic event of floods induced by the breaching of a dyke is rather complicated to predict, not only because it is related to flood water propagation, but also to sediment transport which is still not well understood. In recent years, several small-scale experimental studies and field observations have been investigated to further understand the dyke breach process caused by flow-overtopping (Chinnarasri et al. 2003, Coleman et al. 2002, Froehlich 2008, Morris et al. 2007). Such laboratory experiments provide insight into the continuous breach growth process. Based on this understanding, numerical models are increasingly attractive and have emerged in large numbers because they are cost-effective and the simulations are not restricted by the spatial-scale of flood events.

Traditionally dyke collapse is assumed to be a “sudden dam-break” of the whole structure or a constant breach size. However, such treatments are unrealistic in reality and the “sudden collapse” hypothesis is too conservative. In fact, the dyke breach induced by flow-overtopping is a progressive process of water flow-sediment transport interaction. This progressive rather than sudden erosion delays the onset of the flood, changing the outflow hydrograph. Dam breach models have been classified into different groups by researchers (Singh 1996, Wu et al. 2011), with each kind identified as having advantages and disadvantages as a result of its assumptions or simplifications. The first type of model is the so-called parametric or empirical model which assumes the dyke breach enlarges progressively at a constant

[1]PhD Candidate, School of Civil Engineering, University of Leeds, UK. Email: mingfu.guan@hotmail.com.
[2]Professor, School of Civil Engineering, University of Leeds, UK. Email: N.G.Wright@leeds.ac.uk.
[3]Senior Lecturer, School of Civil Engineering, University. of Leeds, UK. Email: P.A.Sleigh@leeds.ac.uk.

downcutting rate (Froehlich 1995, Froehlich 2008, Pierce et al. 2010, Wahl 1998, Walder and Oconnor 1997). This method estimates the peak outflow or breach width by using statistically derived regression equations with a large number of historical parameters for dams and reservoirs. As such, parametric models are very sensitive to the parameters related to the constant downcutting rate and neglect the flow eroding capacity during the dyke breach process. It is thus probable that unrealistic results could occur under certain flow conditions and material properties. More realistic physically-based models have been developed in recent years(Franca and Almeida 2004, Macchione 2008), but many of these make significant simplifications, for example they assume the breach has a certain shape, neglect some characteristics of the dyke or simply transpose the classical sediment transport equation to describe the breach evolution, all of which limit their application to real cases. More recently 1D and 2D morphodynamic models have been presented based on shallow water theory focusing on embankment breach process and bank erosion issues (Cao et al. 2011, Faeh 2007, Pontillo et al. 2010, Roelvink et al. 2009, Spinewine et al. 2002, Volz et al. 2012). Two-layer models and two-phase models for high concentration sediment-laden flow (Greco et al. 2012, Zech et al. 2008) are also becoming increasingly attractive. However, due to the complexities of dyke breach processes, the detailed breaching models also present some difficulties in application, e.g. the choice of appropriate sediment entrainment function and transport capacity function, as well as how to better model the lateral bed erosion etc. For the dyke breach, bed slope avalanching is certainly a crucial process. In recent years several bank failure operators have been presented in order handle the issues of bank erosion and the dyke breach growth (Spinewine et al. 2002, Swartenbroekx et al. 2010, Volz et al. 2012). Spinewine et al. (2002) suggested, based on experimental evidence, that the critical failure angles should be different above and below the water surface; following this Swartenbroekx et al. (2010) and Volz et al. (2012) developed two-dimensional bank failure operators based on triangular mesh and dual-mesh approaches, respectively.

In this paper, we present a 2D layer-based hydro-morphodynamic model focusing on predicting the flood process caused by a complex dyke breach. An advanced second-order TVD-WAF scheme is proposed to solve the model system numerically and the model is validated by several experimental cases. Further, an easy-to-implement 2D bed slope avalanching model applicable to rectangular meshes is proposed in order to evaluate the stability of bed slope. This is tested by comparing results against two theoretical bed slope failure cases. Due to the irregularity of topography caused by morphological change, the method proposed by (Guan et al. 2013) is used to handle the wetting and drying problem. The model is then applied to an experiment-scale partially breached dyke case.

Morphodynamic model

Model assumptions

Based on an understanding of the physical processes of sheet flow, a layer-based concept divides the whole flow region into an active bed layer; a mixed flow-sediment sheet flow layer and an upper water flow layer (Fig.1). The framework for the layer-based model system considered here consists of:

- a hydrodynamic module governed by the Shallow Water equations with sediment effects;
- a sediment transport module controlling the sediment mass conservation;
- and a bed deformation module for updating the bed elevation under the erosion and deposition of sediment

Flow-sediment interaction is a rather complex process and understanding is still in its infancy; thus it is impossible to include a complete picture of the hydraulic and sedimentary effects accurately in any model. The present model is no exception. Consequently in this work the following assumptions are adopted; (1) the sediment material is considered as non-cohesive for all of the cases studied; (2) the collision effects of sediment particle-particle are ignored; (3) the time scale of bed change is much larger than that of flow movement, thus the flow is calculated assuming a "fixed" bed at each time step.

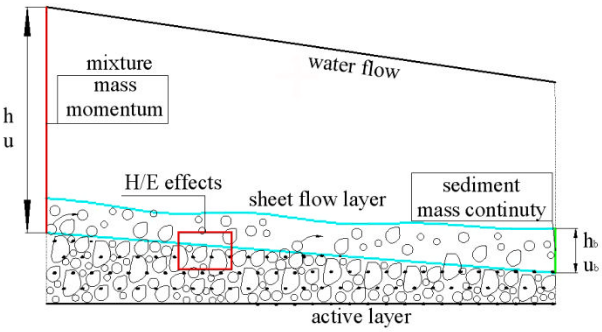

Fig.1. Schematic drawing of the conceptual model in the longitudinal direction

Governing equations

The hydrodynamic model is governed by 2D Shallow Water equations including the mass and momentum exchange between flow and bed. The sediment transport model is governed by the mass conservation of sediment (Li and Duffy 2011, Simpson and Castelltort 2006, Xia et al. 2010). Thus the following equations are used to describe the whole system:

$$\frac{\partial \eta}{\partial t} + \frac{\partial hu}{\partial x} + \frac{\partial hv}{\partial y} = 0 \qquad (1)$$

$$\frac{\partial \rho hu}{\partial t} + \frac{\partial}{\partial x}\rho\left(hu^2 + \tfrac{1}{2}gh^2\right) + \frac{\partial \rho huv}{\partial y} = \rho gh\left(S_{ox} - S_{fx}\right) \qquad (2a)$$

$$\frac{\partial \rho hv}{\partial t} + \frac{\partial \rho huv}{\partial x} + \frac{\partial}{\partial y}\rho\left(hv^2 + \tfrac{1}{2}gh^2\right) = \rho gh\left(S_{oy} - S_{fy}\right) \qquad (2b)$$

$$\frac{\partial h_b C_b}{\partial t} + \frac{\partial h_b u_b C_b}{\partial x} + \frac{\partial h_b v_b C_b}{\partial y} = -\frac{(q_b - q_{b*})}{L} \qquad (3)$$

where η=water surface elevation (m); h=flow depth (m); u, v=average flow velocity in x and y direction (m/s); h_b, u_b, v_b, C_b are depth (m), velocity in x direction (m/s), velocity in y direction (m/s) and volumetric concentration (dimensionless) in sheet flow layer; q_b=real transport rate (m^2/s); q_{b*}= transport capacity (m^2/s); L=non-equilibrium adaptation coefficient of sediment transport (m); ρ=density of sediment and water mixture (m^3/s), $\rho=\rho_w(1-C)+\rho_s C$; C=volumetric concentration in flow depth (dimensionless) ρ_s, ρ_w =density of sediment and water respectively (m^3/s). S_{ox}, S_{oy} are the bed slopes in x and y direction expressed by $S_{ox} = -\frac{\partial z_b}{\partial x}$, $S_{oy} = -\frac{\partial z_b}{\partial y}$; S_{fx}, S_{fy} are the frictional slopes in x and y direction calculated by $S_{fx} = \frac{n^2 u\sqrt{u^2+v^2}}{h^{4/3}}$; $S_{fy} = \frac{n^2 v\sqrt{u^2+v^2}}{h^{4/3}}$. As the mass flux of sediment transport has, say $huC = h_b u_b C_b \rightarrow h_b C_b = \frac{u}{u_b} hC = \beta hC$ in x direction, the Eq.(3) can be approximately converted to the expression below by expanding the Eq.(3):

$$\frac{\partial hC}{\partial t} + \frac{1}{\beta}\frac{\partial huC}{\partial x} + \frac{1}{\beta}\frac{\partial hvC}{\partial y} = -\frac{1}{\beta}\frac{(q_b - q_{b*})}{L} \qquad (4)$$

where $\beta=u/u_b$ is the flow-to-sediment velocity ratio. Also, the relationship $\rho=\rho_w(1-C)+\rho_s C$ is substituted into Eqs.(2) which is then re-formulated. The converted momentum conservation equation is then approximately rewritten as

$$\frac{\partial hu}{\partial t} + \frac{\partial}{\partial x}\left(hu^2 + \frac{1}{2}gh^2\right) + \frac{\partial}{\partial y}huv = gh\left(S_{ox} - S_{fx}\right) + \frac{\Delta\rho u}{\rho}\frac{\partial z_b}{\partial t}\left(\frac{1-p}{\beta} - C\right) - \frac{\Delta\rho g h^2}{2\rho}\frac{\partial C}{\partial x} - S_A \qquad (5a)$$

$$\frac{\partial hu}{\partial t} + \frac{\partial}{\partial x}huv + \frac{\partial}{\partial y}\left(hv^2 + \frac{1}{2}gh^2\right) = gh\left(S_{oy} - S_{fy}\right) + \frac{\Delta\rho v}{\rho}\frac{\partial z_b}{\partial t}\left(\frac{1-p}{\beta} - C\right) - \frac{\Delta\rho g h^2}{2\rho}\frac{\partial C}{\partial y} - S_B \qquad (5b)$$

The morphological evolution is calculated according to the relation of the sediment transport rate and the transport capacity as

$$(1-p)\frac{\partial z_b}{\partial t} = \frac{(q_b - q_{b*})}{L} \tag{6}$$

where p=sediment material porosity (dimensionless); z_b=bed elevation (m); $\Delta\rho=\rho_s-\rho_w$; S_A, S_B are the additional terms related to the velocity ratio β which is expressed by

$$S_{A,B} = \frac{\Delta\rho V}{\rho}\left(1-\frac{1}{\beta}\right)\left[\left(C\frac{\partial hu}{\partial x} + C\frac{\partial hv}{\partial y}\right) - \left(hu\frac{\partial C}{\partial x} + hv\frac{\partial C}{\partial y}\right)\right]$$

where U=u for S_A; U=v for S_B; The last three source terms of Eqs.(5a-b) represent the interaction effects of sediment and water flow and momentum transfer due to sediment exchange.

Empirical relationships

Threshold for incipient motion

The threshold of sediment incipient motion is closely related to the dimensionless sediment particle size. The relationship proposed by Soulsby (Soulsby 1997) is applied in this paper.

$$\theta_c = \frac{0.30}{1+1.2d^*} + 0.055[1-\exp(-0.02d^*)] \tag{7}$$

in which, $d^*=d[(s-1)g/v^2]^{1/3}$ represents the dimensionless sediment particle size. With consideration of bed slope effects, the critical dimensionless bed shear stress is calculated by

$$\theta_{cr} = k_1\theta_c \tag{8}$$

where θ_{cr} is the critical dimensionless bed shear stress for sediment incipient motion; k_1 is the coefficient corresponding to bed slope effects. Based on the investigation of Smart and Jäggi (Smart and Jäggi 1983), k_1 is determined according to the relation of flow direction and bed slope S as

$$k_1 = \begin{cases} \cos(\arctan\ |S_{ox}|)(1-|S_{ox}|/\tan\varphi) & u\cdot S_{ox} < 0 \\ \cos(\arctan\ |S_{ox}|)(1+|S_{ox}|/\tan\varphi) & u\cdot S_{ox} > 0 \end{cases}$$

where φ is the angle of repose; u, S_{ox} are the velocity and the bed slope in x direction; similar equations can be derived for the y direction.

The flow-to-sediment velocity ratio

The sheet flow velocity has been studied by the derivation of empirical relationships based on experiments (Greimann et al. 2008, Hu and Hui 1996, van Rijn 1984). In this paper, the Eqn. by (Greimann et al. 2008) is used to estimate the approximate velocity ratio. In terms of high bed shear stress with $\theta\geq 20\theta_{cr}$, the flow-to-sediment velocity ratio β=1 is assumed. Thus

$$\beta = \begin{cases} \frac{u}{u_b} = \frac{u}{u_*}\frac{\sqrt{\theta_{cr}}}{1.1(\theta/\theta_{cr})^{0.17}[1-\exp(-5\theta/\theta_{cr})]} & \theta/\theta_{cr} < 20 \\ 1 & \theta/\theta_{cr} \geq 20 \end{cases} \tag{9}$$

where θ is the real dimensionless bed shear stress.

Non-equilibrium adaptation coefficient L

The non-equilibrium adaptation length L means the ability of sediment particles movement in water flows. The coefficient L has been investigated by many researchers (Armanini and Di Silvio 1988, Greimann et al. 2008, Wu 2004), following which, the relationship $L = h\sqrt{u^2+v^2}/\gamma\omega$ is used, but the coefficient γ is regarded as the ratio of the near-bed concentration and the volumetric concentration in flow with a maximum of (1-p). Thus,

$$L = \frac{h\sqrt{u^2+v^2}}{\gamma\omega} \text{ with } \gamma = \min\left(\frac{C_b}{C}, \frac{1-p}{C}\right) = \min\left(\alpha\frac{h}{h_b}, \frac{1-p}{C}\right)$$

in which, $h_b=\mu\theta d_{50}$, μ is a dimensionless coefficient ranging from 6 to 12 related to sediment material that depends on sediment setting velocity (Pugh and Wilson 1999, Sumer et al. 1996); ω is the effective settling velocity of sediment determined by Soulsby's equation (Soulsby 1997); α is the sediment-to-flow velocity ratio determined by Eq.(9).

Sediment transport rate

The commonly-used relationship, Meyer-Peter & Müller equation (*MPM*) (Meyer-Peter and Müller 1948), is adopted. However, the *MPM* equation is derived for bed load transport based on the experiment data for bed slope from 0.0004 to 0.02 and dimensionless bed shear stress smaller than 0.25. Therefore, in this study, *MPM* is applied only for gentle bed slope of <0.03 and a calibrated coefficient ψ is incorporated to modify the equation. The modified sediment transport rate is (*M_MPM*) expressed by:

$$q_{b*} = \psi 8(\theta-\theta_{cr})^{1.5}\sqrt{(s-1)gd_{50}^3} \quad 0 \le S_o < 0.03\ (M\_MPM)$$

where ψ is a calibrated coefficient. With respect to bed slopes of ≥0.03, Smart and Jäggi (Smart and Jäggi 1983) expanded the database obtained by *MPM* for the steep slope range up to 0.03-0.20. They performed flume experiments to estimate the maximum transport capacity of mountain streams given by the equation below. However, for the case of bed slope>0.2, the bed slope S is modified to be 0.2 in the equation to avoid the calculated transport rate being un-physically large due to surpassing the limitation range of bed slope. The slightly modified equation (*M_SJ*) can be written by:

$$q_{b*} = 4\left(\frac{d_{90}}{d_{30}}\right)^{0.2}\frac{h^{1/6}}{n\sqrt{g}}\min(S_o, 0.2)^{0.6}\,\theta^{0.5}(\theta-\theta_{cr})\sqrt{(s-1)gd_{50}^3 S_o} \ \ge 0.03\ (M\_SJ)$$

in which, d_{90}/d_{30}=1.02 for uniform sediment particles.

Two-dimensional bed slope avalanching model

As discussed in the introduction, Swartenbroekx et al. (2010) and Volz et al. (2012) have developed two-dimensional bank failure operators using different critical angles above and below the water; however, both of these approaches are presented for triangular meshes and these equations are not applicable to Cartesian cells. In this section, an easy-to-implement 2D bed slope avalanching model is proposed for application on rectangular meshes. The principle of this method is that: if the bed slope φ_i of a non-cohesive bed becomes steeper than the critical angle of failure φ, the bed avalanching will then occur to form a new bedform with a slope approximately equal to the critical angle of repose. In short, the process of avalanching is simulated by enforcing $|\varphi_i|\le\varphi$, while maintaining mass conservation of sediment material. As shown in Fig.2. for the discretisation of rectangular cells in two dimensions, there are eight cells surrounding each cell. Taking, say cell (i, j); bed slope avalanching may occur in four directions (direction 1, 2, 3 and 4) will be used for updating the elevation in cell (i, j). Correspondingly, the avalanching approach is divided into four steps in the four directions, and each update of bed level at cell (i, j) is based on the calculation in the previous step.

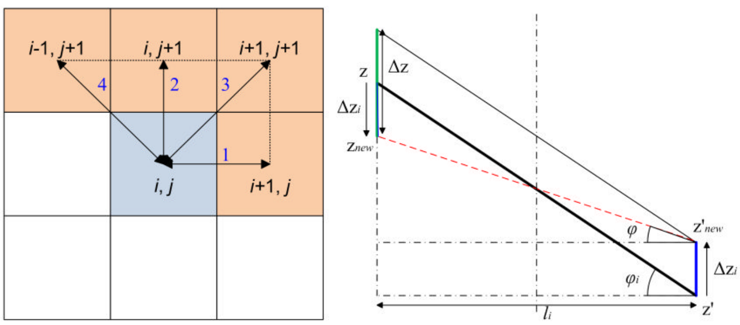

Fig.2. Schematic diagram of proposed bed level updating; (*a*) the re-form process in two dimensions; (b) the updating of two adjacent computational cells in *i* direction

We take the re-forming process of sediment in i (i=1, 2, 3, 4) direction as an example to derive the updating equation as follows. When $\varphi_i > \varphi$, the new angle of bed slope is approximately equal to the angle of repose by reducing the higher cell elevation and elevating the lower cell elevation. This is depicted in Fig.1for the case of $\varphi_i > 0$, in which case Δz_i is calculated using:

$$\Delta z_i = \frac{\Delta z}{2} \approx \frac{l_i(\tan\varphi_i - \tan\varphi)}{2} \tag{10}$$

where l_i = the length of two cells in i direction; $l_1 = dx$; $l_2 = dy$; $l_3 = l_4 = \sqrt{dx^2 + dy^2}$. As the bed slope angle φ_i in i (i=1, 2, 3, 4) direction might be negative or positive, the equation above is rewritten with consideration of the positive and negative of φ_i by

$$\Delta z_i = \begin{cases} \frac{\Delta z}{2} \approx sign(\varphi_i)\frac{l_i(\tan|\varphi_i| - \tan\varphi)}{2} & |\varphi_i| > \varphi \\ 0 & |\varphi_i| \le \varphi \end{cases} \quad where \;\; sign(a) = \begin{cases} 1 & a > 0 \\ 0 & a = 0 \\ -1 & a < 0 \end{cases} \tag{11}$$

Thus, the modified 2D bed slope avalanching equation is finally given by

$$\begin{cases} z_{new(i,j)} = z_{i,j} + \sum_{i=1}^{4} \Delta z_i \\ z_{new(i,j+1)} = z_{i,j+1} - \Delta z_1 \\ z_{new(i+1,j)} = z_{i+1,j} - \Delta z_2 \\ z_{new(i+1,j+1)} = z_{i+1,j+1} - \Delta z_3 \\ z_{new(i-1,j+1)} = z_{i-1,j+1} - \Delta z_4 \end{cases} \tag{12}$$

Since avalanching between two cells may induce new avalanching at neighbouring cells, the sweeping process is repeated using Eq.(12) until no further avalanching occurs. The re-forming process is however time-consuming which considerably increases the computational time. In general, the time step of bed slope avalanching depends on the sediment material properties closely and it is difficult to estimate it. In this study, to increase simulation efficiency, the stability analysis is implemented at a larger time step based on a sensitivity test which shows an insignificant influence of it on the predicted results. Additionally, different values are used for the critical angles (φ_{dc} for dry bed and φ_{wc} for wet bed) and the re-formation bed slope angles (φ_{dr} for dry bed and φ_{wr} for wet bed) above and below the water as supported by (Spinewine et al. 2002). Here, the wet and dry conditions are evaluated according to the simulated value of water depth at each time step. Correspondingly, the estimated critical and re-formation bed slope angles are assigned for the two different conditions.

Numerical Solution

Eq.(1), Eq.(2) and Eq.(3) constitute a shallow water non-linear system. In compact form, the governing equations can be expressed by

$$\frac{\partial \mathbf{U}}{\partial t} + \frac{\partial \mathbf{F}}{\partial x} + \frac{\partial \mathbf{G}}{\partial y} = \mathbf{S} \tag{13}$$

$$\mathbf{U} = \begin{bmatrix} \eta \\ hu \\ hv \\ hC \end{bmatrix}, \mathbf{F} = \begin{bmatrix} hu \\ hu^2 + \frac{1}{2}gh^2 \\ huv \\ \frac{1}{\beta}huC \end{bmatrix}, \mathbf{G} = \begin{bmatrix} hu \\ huv \\ hv^2 + \frac{1}{2}gh^2 \\ \frac{1}{\beta}hvC \end{bmatrix}, \mathbf{S} = \begin{bmatrix} 0 \\ gh(S_{ox} - S_{fx}) + \frac{\Delta\rho u}{\rho}\frac{\partial z_b}{\partial t}\left(\frac{1-p}{\beta} - C\right) - \frac{\Delta\rho g h^2}{2\rho}\frac{\partial C}{\partial x} - S_A \\ gh(S_{oy} - S_{fy}) + \frac{\Delta\rho v}{\rho}\frac{\partial z_b}{\partial t}\left(\frac{1-p}{\beta} - C\right) - \frac{\Delta\rho g h^2}{2\rho}\frac{\partial C}{\partial y} - S_B \\ -\frac{1}{\beta}\frac{(q_b - q_{b*})}{L} \end{bmatrix}$$

To solve the system (13), a HLL based scheme has been used. An excellent description of this approach is given by Toro (Toro 2001), so a detailed description is omitted here. However, the proposed model system incorporates an extra governing equation for sediment transport. To incorporate this in to the HLL Riemann solver, the flux at the interface of two adjacent cells is obtained by the use of a middle contact discontinuity waves S_*. Through the assessment of S_*, the sediment flux is determined based on the concentration at the right cell or left cell. In the following, a brief description is given explaining how this interface flux is calculated for the coupled flow and sediment model. Firstly, the first three flux terms can be expressed by the basic HLL scheme expression as follows:

$$\mathbf{E}^{*}_{LR\ 1,2,3} = \begin{cases} \mathbf{E}_L & if\ S_L \geq 0 \\ \mathbf{E}_R & if\ S_R \leq 0 \\ \mathbf{E}^{*} & otherwise \end{cases} \tag{14}$$

where $\mathbf{E}_L$ =$\mathbf{E}(\mathbf{U}_L)$, $\mathbf{E}_R$ =$\mathbf{E}(\mathbf{U}_R)$ are the flux and conservative variable vectors at the left and right side of each cell interface. $\mathbf{E}^{*}$is the numerical flux in the star region, calculated in two dimensions by

$$\mathbf{E}^{*} \cdot \mathbf{n} = \frac{S_R \mathbf{E}_L \cdot \mathbf{n} - S_L \mathbf{E}_R \cdot \mathbf{n} + S_R S_L (\mathbf{U}_R - \mathbf{U}_L)}{S_R - S_L}$$

in which, $\mathbf{n}=[n_x,\ n_y]^{\mathrm{T}}$; the S_L and S_R denote two wave speeds which must be selected carefully to avoid any entropy violation. The so-called "two expansion" approach (Toro 1992) was adopted here including dry-bed options to estimate S_L and S_R. They are expressed by

$$S_L = \begin{cases} \min\left(\mathbf{q}_L \cdot \mathbf{n} - \sqrt{g h_L}, u^{*} - \sqrt{g h^{*}}\right) & if\ h_L > 0 \\ \mathbf{q}_R \cdot \mathbf{n} - 2\sqrt{g h_R} & if\ h_L = 0 \end{cases};\ S_R = \begin{cases} \min\left(\mathbf{q}_R \cdot \mathbf{n} + \sqrt{g h_R}, u^{*} - \sqrt{g h^{*}}\right) & if\ h_R > 0 \\ \mathbf{q}_L \cdot \mathbf{n} + 2\sqrt{g h_L} & if\ h_R = 0 \end{cases}$$

where $u^{*} = \frac{1}{2}(\mathbf{q}_L + \mathbf{q}_R) \cdot \mathbf{n} + \sqrt{g h_L} - \sqrt{g h_R}$, $\sqrt{g h^{*}} = \frac{1}{2}\left(\sqrt{g h_L} + \sqrt{g h_R}\right) + \frac{1}{4}(\mathbf{q}_L - \mathbf{q}_R) \cdot \mathbf{n}$; $\mathbf{q}=[u,\ v]$. The middle wave speed $S_*$is calculated by the following form as recommended by Toro (2001).

$$S_* = \frac{S_L h_R (\mathbf{q}_R \cdot \mathbf{n} - S_R) - S_R h_L (\mathbf{q}_L \cdot \mathbf{n} - S_L)}{h_R (\mathbf{q}_R \cdot \mathbf{n} - S_R) - h_L (\mathbf{q}_L \cdot \mathbf{n} - S_L)}$$

To calculate the intercell numerical fluxes, a weighted average flux (WAF) of total variation diminishing (TVD) method is employed with a flux limiter function. The TVD-WAF scheme is second-order accurate in space and time by solving the conventional Riemann problem associated with the first-order Godunov scheme. A detailed description can be found in (Toro, 2001). Taking the calculation of flux in the x direction as an example, this is calculated using:

$$\mathbf{F}^{*}_{i+1/2,(1,2,3)} = \frac{1}{2}(\mathbf{F}_i + \mathbf{F}_{i+1}) - \frac{1}{2}\sum_{k=1}^{N} sign(c_k) \Phi^{k}_{i+1/2} \Delta \mathbf{F}^{k}_{i+1/2} \tag{15}$$

in which, $\mathbf{F}_i$= $\mathbf{F}(\mathbf{U}_i)$, $\mathbf{F}_{i+1}$= $\mathbf{F}(\mathbf{U}_{i+1})$ are the flux and conservative variable vectors at the left and right sides of each cell interface; c_k is the Courant number for wave k, $c_k=\Delta t S_k/\Delta x$; S_k is the speed of wave k and N is the number of waves in the solution of the Riemann problem, N=2 in conjunction with HLL approximate Riemann solver. $\Delta\mathbf{F}^{(k)}_{i+1/2}$=$\mathbf{F}^{(k+1)}_{i+1/2}$-$\mathbf{F}^{(k)}_{i+1/2}$, which is the flux jump across wave k; $\mathbf{F}^{(k)}_{i+1/2}$ is the value of the flux vector in the interval k; herein $\mathbf{F}^{(1)}_{i+1/2}$=$\mathbf{F}(\mathbf{U}_L)$, $\mathbf{F}^{(2)}_{i+1/2}$=$\mathbf{F}(\mathbf{U}^{*})$, and $\mathbf{F}^{(3)}_{i+1/2}$=$\mathbf{F}(\mathbf{U}_R)$ which are estimated by virtue of the HLL approximate Riemann solver, $\Phi(r)$ is the WAF limiter function. The WAF limiter used here is expressed through the well-known conventional flux limiter term $\varphi(r)$ was the *min*-mod limiter:

$$\Phi(r) = 1-(1-|c|)\varphi(r) \text{ with } \varphi(r)=\max[0,\ \min(1,\ r)] \quad (\textit{min}\text{-mod limiter})$$

where $r^{(k)}$ is the ratio of the upwind change to the local change in scalar quantity q. It can be written by:

$$r^{(k)} = \begin{cases} \Delta q^{(k)}_{i-1/2} / \Delta q^{(k)}_{i+1/2} = \left(q^{(k)}_{i} - q^{(k)}_{i-1}\right) / \left(q^{(k)}_{i+1} - q^{(k)}_{i}\right) & if\ c_k > 0 \\ \Delta q^{(k)}_{i-3/2} / \Delta q^{(k)}_{i+1/2} = \left(q^{(k)}_{i+2} - q^{(k)}_{i+1}\right) / \left(q^{(k)}_{i+1} - q^{(k)}_{i}\right) & if\ c_k > 0 \end{cases}$$

For the x split 2D Shallow Water equations we choose $q=\eta$ for the left wave S_L (k=1) and the right wave S_R (k=2). Based on the solution of the previous three flux terms, the fourth flux term-sediment flux $F_{i+1/2,4}$ at the interface of two adjacent cells is determined by the relationship of the middle waves S_* and zero, calculated by

$$F^{*}_{i+1/2,4} = \begin{cases} F^{*}_{i+1/2,1} C_L & S_* \geq 0 \\ F^{*}_{i+1/2,1} C_R & S_* < 0 \end{cases} \tag{16}$$

where C_L and C_R are the volumetric sediment concentration in left and right cells; $F_{i+1/2,1}$ is the first flux component calculated by Eq.(15). Furthermore, the source term and wetting/drying are treated by using the method published in (Guan et al. 2013). The numerical scheme is explicit, so for stability the Courant-Friedrichs-Lewy ($0<CFL<1$) stability condition must be applied to limit the time step Δt.

Validation of morphodynamic model

Unstable bed failure

Two theoretical tests were undertaken to validate the proposed bed slope avalanching model. The first is to test bank failure in a square channel with vertical banks. The inlet and outlet of the channel are assumed to be glass walls. Initially, the bank elevation is 4m and the static water level in the channel is 1.5m. The critical failure angles of wet bed and dry bed are considered as 61° and 31° respectively, and the reformation angle of both are 60° and 30° respectively. Fig.3a illustrates the topography of channel after applying the bed slope avalanching model. It is shown that the final stable bank slopes above and below the water are equal to the corresponding critical angles. Test 2 examines the spatial behaviour of the avalanching model. A half-oval dune was placed in the centre of a completely dry bed (Fig.3b). The failure angles were assumed to be 40°. In the simulation, the unstable side walls were flattened towards the circle and an approximately symmetrical cone-shaped configuration formed. The applicability of the geometrical approach was demonstrated in both tests and mass continuity was maintained despite the large mass movements.

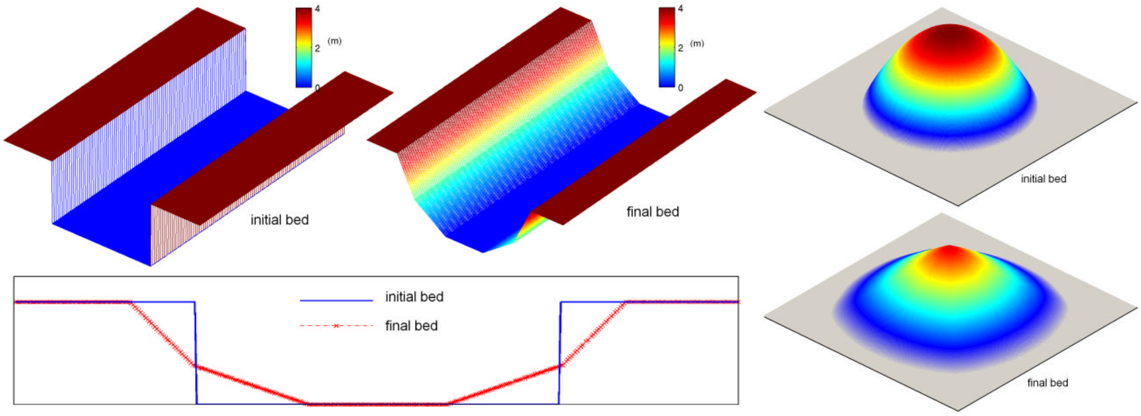

Fig.3. Tests for bed slope avalanching; left: vertical bed with water pool; right: circle dune

Unsteady dam-break flow over movable bed

Experiments of a dam-break flow over movable bed were conducted using PVC pellets and sand as the bed material in the laboratory of UCL in Belgium. Details of these can be found in (Fraccarollo and Capart 2002). The purpose of these tests, which are a 1D case but implemented in 2D, was to elucidate the applicability of the morphodynamic model in an unsteady outburst flow. The case of cylindrical PVC pellets was chosen; the parameters of PVC particles include: the equivalent spherical diameter is 3.5mm, the density is 1540kg/m^3, the sediment material porosity p=0.47, and the settling velocity is about 18cm/s according to the experiment. The experiments were implemented in a horizontal prismatic flume with a rectangular cross section of $2.5m\times0.1m\times0.25m$. This case is simulated by applying first-order HLL solver, first-order Roe solver, second-order TVD-WAF scheme and TVD-Lax-Wendroff in order to evaluate the effect of the solver's accuracy on the results. Fig.4 shows that the numerical model simulates the temporal evolution of erodible bed effectively; and that the water level and bed scour is predicted with good agreement although there are some slight differences in terms of bed scour depth and water level. Moreover, the comparison indicates that the scheme's formal numerical accuracy does not significantly influence the model results. Following this result the attractive second-order TVD-WAF scheme is adopted in all cases discussed in the rest of this paper. This was chosen as it has been well tested, is robust and is easy to implement (Guan et al. 2013).

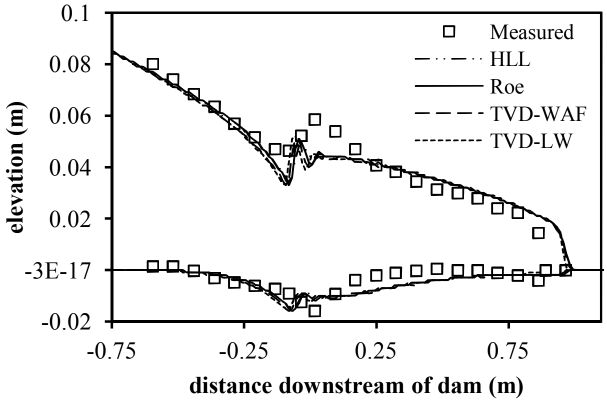

Fig.4. Comparison between measured data and simulated results at t=10t^0 (t^0=0.101s) for dam-break flow over movable bed test

Dam-break flow in an erodible channel with a sudden enlargement

To verify the capability of the morphodynamic model in a two-dimensional domain, the experimental test investigated in the laboratory of UCL in Belgium (Goutiere et al. 2011) is reproduced here. The initial experimental setup is shown in Fig.4. The initial water depths before and after the gate are 0.25m and 0m respectively; the erodible bed layer is set at 0.1m thick and consists of fully saturated sand with an uniformity index of d_{84}/d_{16}=1.96 and a median diameter of 1.72mm. The density of sand is 2.63×10^3kg/m^3, and the sediment porosity is 39%. The downstream outlet is an open free outfall and the sediment bed is maintained at the initial elevation by a vertical plate presenting the same height as the bed layer. For the simulation, the model domain was discretised by 300×100 uniform cells. As suggested by the experimental work the Manning's coefficient is set to be equal to 0.023, the calibration coefficient ψ is equal to 1.0 and the dimensionless coefficient μ is set to be 9.0.

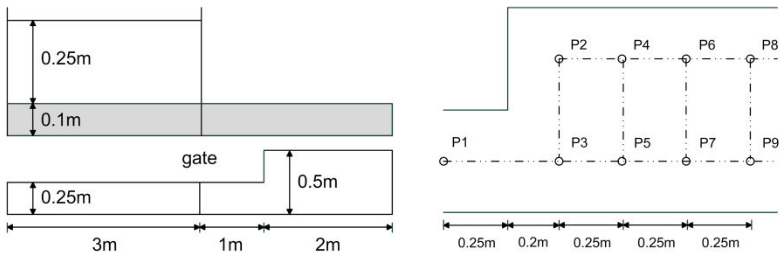

Fig.5. Sketch of a dam-break flow experiment over a mobile bed

In order to validate the performance of the model a comparison of the simulated water level and the measured data against the time at the measured gauges of P1, P2, P5 and P6 is shown in Fig.6. This indicates that the simulated water level agrees with the measured data quite well. The flow-sediment interaction process is completed and reaches a stationary state after around 50s. This simulated final bed topography is shown in Fig.7. Compared to the experimental images of the final bed in (Goutiere et al. 2011), the simulated bed shows two similar main characteristic patterns. Firstly, an eroded hole is generated at the enlargement location area where the most severe erosion occurs; the second characteristic area is located near to the left side-wall (facing flow direction) behind the expansion outlet where a deposited mound is predicted. These agree well with the distribution erosion and deposition observed in the experiment. To further elucidate the erodible bed change, the simulated bed profiles at the two cross sections (CS1: 4.2m, CS2: 4.5m downstream from the inlet) are compared with the measured data in Fig.8. In addition, we also illustrate the simulated results by the SWE-Exner model by Soares-Frazão and Zech (Soares-Frazão and Zech 2011) to show the improvement that the present model provides. At the CS2 (x=4.5m), the simulated bed profile by the present model achieves fairly good agreement with the measured cross section, this is much better than the profile simulated by the SWE-Exner model. At CS1(x=4.2m), however, the simulated bed profile is over estimated by the present model in terms of quantitative assessment; there the scour hole moves faster than the experimental observation and the maximum height of the deposited mound is slightly larger than the measured bed. While the trend of the erosion and deposition at the cross section is predicted with a similar shape with the measured bed profile, which is qualitatively better than that simulated by the SWE-Exner model. Possible reasons for the quantitative discrepancy are: firstly, the sediment particle (1.72mm) is very coarse for the water depth (maximum 0.25m), so the particle-particle collision effects, which are neglected by the present model, may be significant; secondly, the effect of the secondary flow at the expansion outlet probably plays a significant role in this particular case.

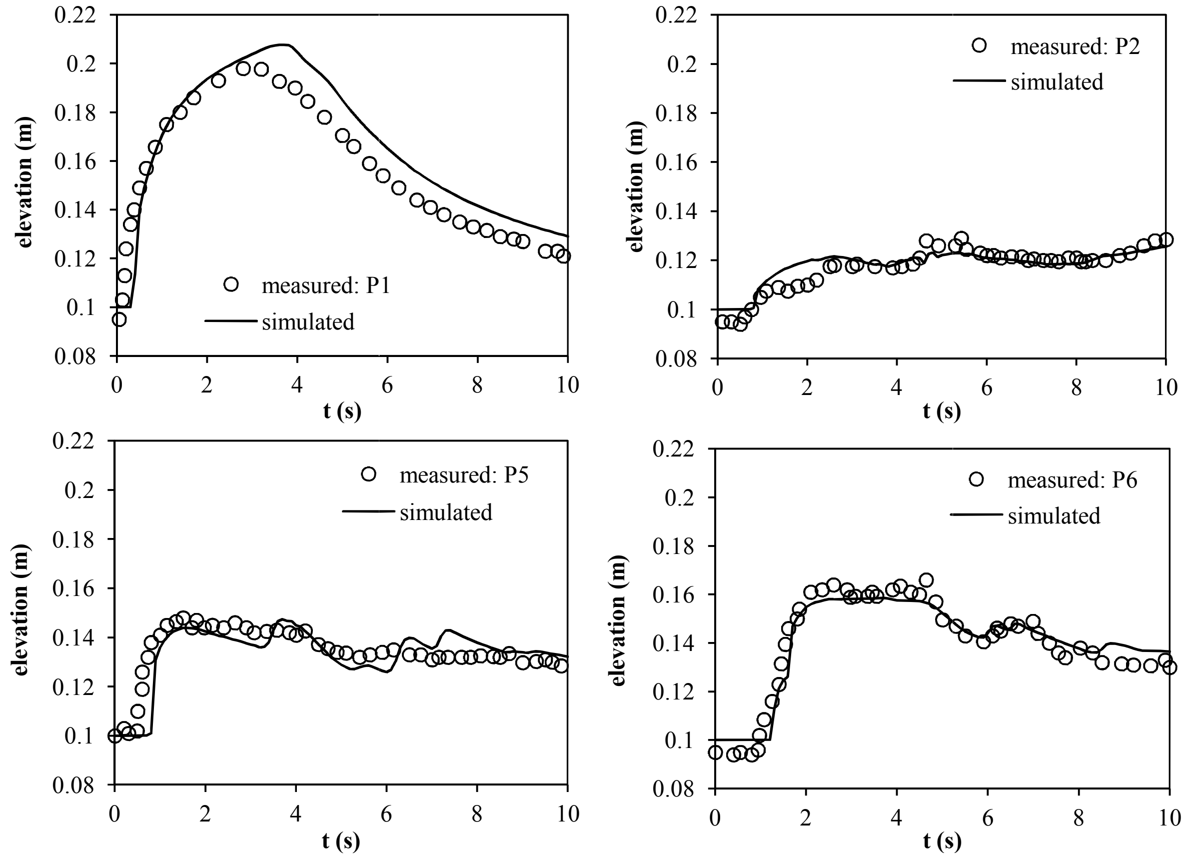

Fig.6. Comparisons between simulated and measured water levels at P1, P2, P5 and P6

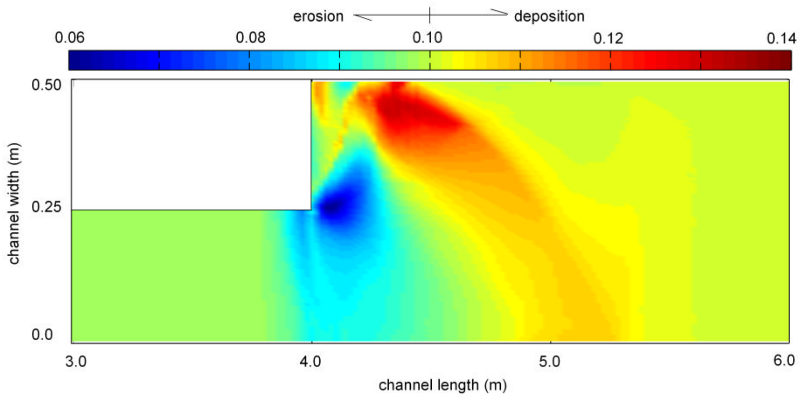

Fig.7. Simulated final bed topography

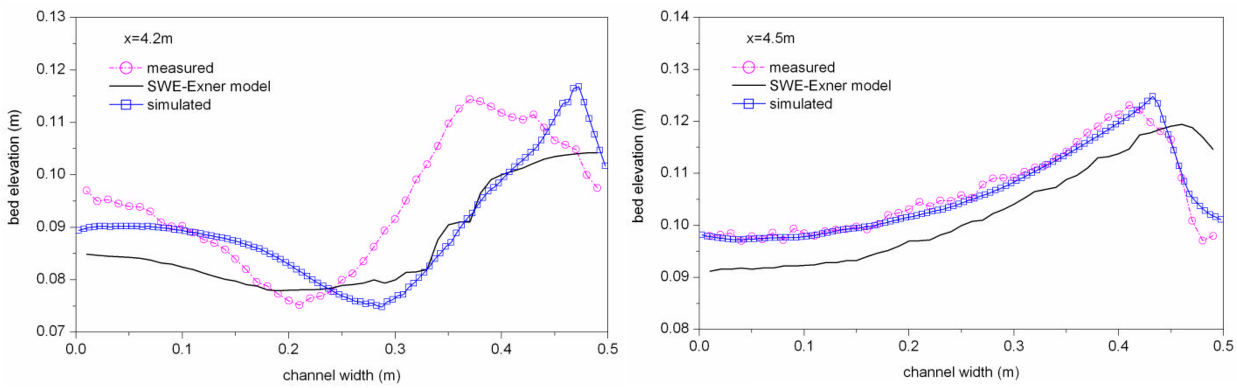

Fig.8. Comparisons between simulated bed profile and measured bed profile at x=4.2m and x=4.5m

Dam erosion due to flow overtopping

Dam erosion due to flow overtopping is a complex flow process involving outburst flow, transition from supercritical flow to subcritical flow and eventually steady flow. This test is presented to verify that the 2D morphodynamic model can predict the erosion and deposition under complex hydraulic conditions. The experiment denoted Run2 conducted by (Chinnarasri et al. 2003)is reproduced here. A dyke was located in the middle of a flume of 35m×1m×1m being 0.8m in height, 1m wide with a crest width of 0.3m. The upstream and downstream slope of the dam was 1V:3H and 1V:2.5H, respectively. The dyke is composed of sand with a median diameter of 1.13mm, and the density of 2.65×10^3 kg/m^3. The initial reservoir level is 0.83m and the downstream water level is 0.03m; the inflow discharge has a constant value of $1.23\times10^{-3} m^3/s$; the bed material porosity is taken as 0.35; the Manning coefficient n is determined as 0.018; the calibration coefficient ψ=1.5 and the dimensionless coefficient μ=9.0 for this case.

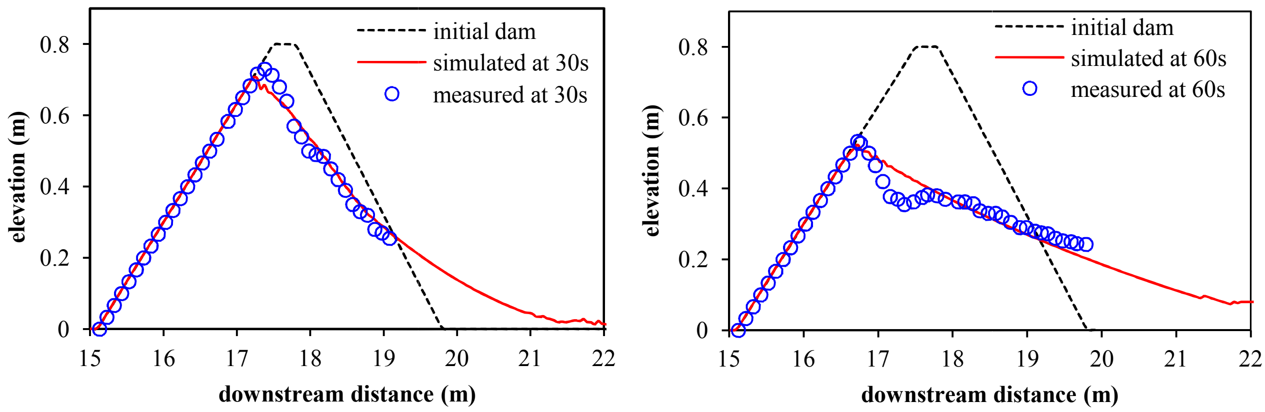

Fig.9. Comparison between simulated dam profile and measured dam profile at t=30s and 60s for full dyke breach test

For the simulation, the area is discretised by 700×10 cells (dx=0.05m, dy=0.1m); the sediment transport rate is calculated by the equation of *M_SJ* and *M_MPM* according to the extent of the bed slope. Fig.9 illustrates the comparison between the simulated dyke bed profiles and measured data at t=30s and t=60s. At 30s the comparison shows fairly good agreement. A reasonably good agreement is also achieved at t=60s, but a larger discrepancy is observed at the top of the dam. A scour hole occurs in the observation, yet this area is smooth in the numerical result. Fig.10 illustrates the comparisons between the simulated results and the measured data: the water level and the outflow discharge. The agreements are again reasonably good, but it also be seen that the simulated water level is slightly lower than the measured data before 90s and that the arrival time of the peak discharge is slightly earlier. The inaccuracies indicated by Fig.9 and Fig.10 are most likely caused by the choice of empirical parameters in the present model, e.g. Manning's coefficient, bed slope effects, empirical sediment transport function etc. Most of the empirical functions are derived based on experimental data and as such are unlikely to be completely applicable to all the complex flow conditions. We have performed a simulation on a finer mesh, and found that the mesh size is not a major reason causing the inaccuracies.

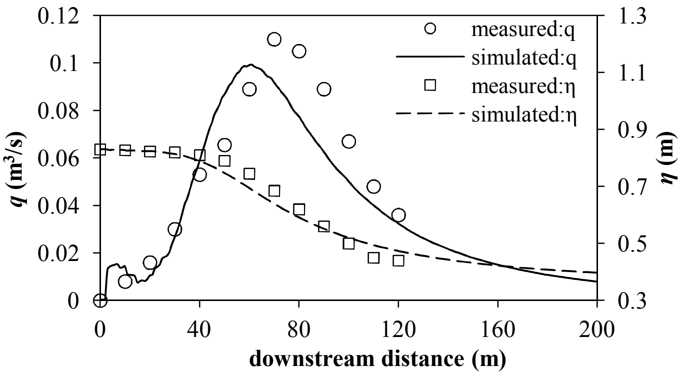

Fig.10. Comparisons between simulated results and measured data for full dyke breach test

Simulation of a Dyke Breach from a Partial Overtopping Flow

In this section, a flood event caused by a partially breached dyke is reproduced by the validated morphodynamic model to simulate the spatial and temporal evolution of the dyke breach. The predicted outflow hydrograph and the change of water level in the reservoir are compared with measured data.

Experimental conditions

The experiment conducted by UCL (Spinewine et al. 2004) was simulated. A sand dyke of 2.4*m* long and 0.47*m* high was built at 11.8*m* along a 36.2*m*×3.6*m* flume; two fixed blocks were placed on the left and right sides of the dyke; the upstream and downstream slopes of sand dyke were 1:2 and 1:3 respectively, and a 10*cm* sand layer was laid downstream of the dam. The sediment material was composed of sand with a median diameter d_{50}=1.80*mm*, specific gravity of s=2.615 and a loose bed porosity p=0.42 after compaction. An upstream reservoir contained water for the experiment, which was held by a gate which was then gradually opened so the water filled the region upstream of the dyke until water level was at 0.45*m*. A small trapezoidal breach was dug on the top middle of dyke to initiate the flow overtopping at this point. Subsequently the breach enlarged with the flow gradually with increasing time. The two blocks besides the sand dike are treated as the part of the sand dyke with the restriction that in the simulation they are not erodible.

Measured data

The measured data (Spinewine et al. 2004) used is:

(1) the water level change with time in the upstream reservoir;

(2) the outflow discharge against time;

(3) full digital terrain models (DTMs) of the breach topography interpolated from laser-observed transverse profiles.

The outflow discharge was estimated by using the measured water level, thus the estimated outflow hydrographs show a significant uncertainty range as shown in (Spinewine et al. 2004, Van Emelen et al. 2011); the estimated discharge Q2 is used in the following.

Predicted hydrograph

The whole dyke and channel are discretised with dx=0.035*m* and dy=0.03*m* and the coefficient values ψ=1.5 and μ=9.0 were chosen. For this kind of flood event the outflow peak discharge is a vital hydraulic parameter that needs to be predicted. Manning's coefficient *n* has a direct influence on the bed shear stress and thus strongly influences the flow-induced sediment transport; therefore, four different Manning's coefficients (*n*=0.017, 0.018, 0.019, 0.02) are used for evaluating and analysing its sensitivity in the modelling of the dyke breach process. Fig.10 illustrates the comparisons between the predicted results and the measured data, showing both the outflow hydrograph (Fig.11a) and the water level in the reservoir (Fig.11b). It can be seen that the Manning's coefficient changes the peak value and the time of occurrence of the peak outflow discharge, consequently the water level in the reservoir is also affected. More specifically, the larger the Manning's coefficient the more water flow from the reservoir, thus the outflow peak discharge becomes larger and occurs at an earlier time. The reason for this is primarily because increasing Manning's coefficient increases the calculated bed shear stress, so the dyke is eroded more severely and thereby the breach process is accelerated. Some small oscillations occur at the simulated outflow hydrograph, in particular at the peak stage. These occur because the lateral bed avalanching erodes the sediment material of the breach, which raises the elevation of the breach temporarily and locally blocks the flow; then as further erosion occurs based on the previous updating of the bed. Overall, the present model predicts the outflow hydrograph and the temporal change of water level in the reservoir effectively with good agreement to measured data.

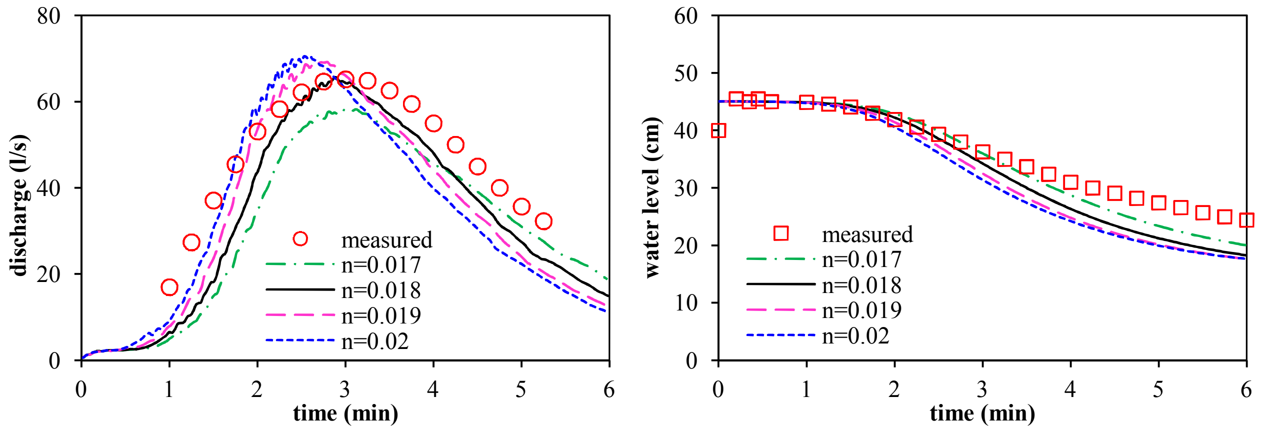

Fig.11. Comparisons between predicted result and measured data for partial dyke breach test, (a) water level; (b) outflow discharge

Simulated dyke breach

As mentioned above, the DTMs (Spinewine et al. 2004, Van Emelen et al. 2011) are compared with the simulated dyke terrain to assess the capability of the present model and the bed slope avalanching model to predict the breach size. The DTMs themselves suffer from a lack of accuracy in certain regions because of air/water refraction issues and water covered land when the measurements were taken. For the simulation, n=0.018 is chosen because the model reproduced the peak discharge accurately at this value. Fig.12 displays the digital terrain measurements compared to the simulated dyke breach at the initial stage t=20s and the final stage t=370s. The breaching process is reasonably well reproduced. The numerical model predicts slightly more severe erosion at the downstream toe of the dyke at t=20s; it is clear that more deposition is indicated there by the digital terrain data. At t=370s, more severe erosion can be observed in the middle area of the dyke, whilst less lateral erosion occurs at each side of the breach. The sediment transport model appears to overestimate the vertical erosion, while the bed slope avalanching model slightly underestimates the lateral erosion presenting a narrower breach. Fig.13 shows the simulated spatial distribution of bed and water in the stretched ordinates, as well as the experimental data at the final equilibrium stage. It can be seen that the present model reproduces the characteristic erosion, deposition and wet/dry areas well; the eroded sediment from the breach primarily deposits behind the dyke and a secondary channel is formed along the centreline. In summary, the present model can reproduce the dyke breach process effectively, while also presenting some shortcomings which need to be addressed when being applied in practice. These shortcomings are:

(1) It is difficult to estimate the empirical parameters for sediment transport which could cause some differences; thus appropriate calibration parameters are necessary for predicting the dyke breach.

(2) The bed slope avalanching occurs based on the consideration of the relationship between the bed slope and the critical angles; hence it does not simulate the lateral random dyke collapse.

(3) The failure time step for the lateral erosion which depends closely on the sediment material properties is difficult to estimate; a sensitivity test was carried out with updating using two different failure time steps. It was seen that this did not influence the final breach size, while the arrival time of the peak discharge has a slight difference.

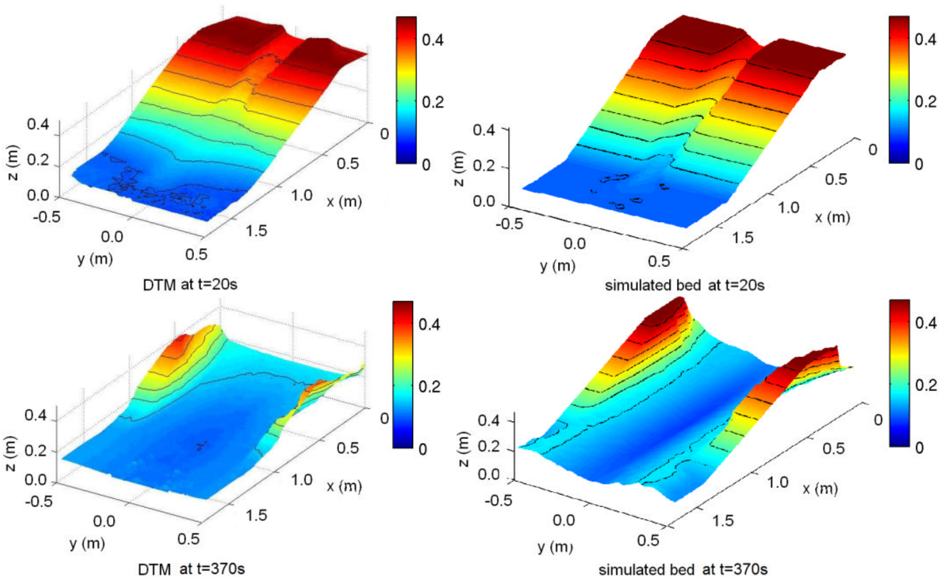

Fig.12. DTM (Van Emelen et al. 2011) and simulated dyke breach due to flow overtopping at t=20s and 370s

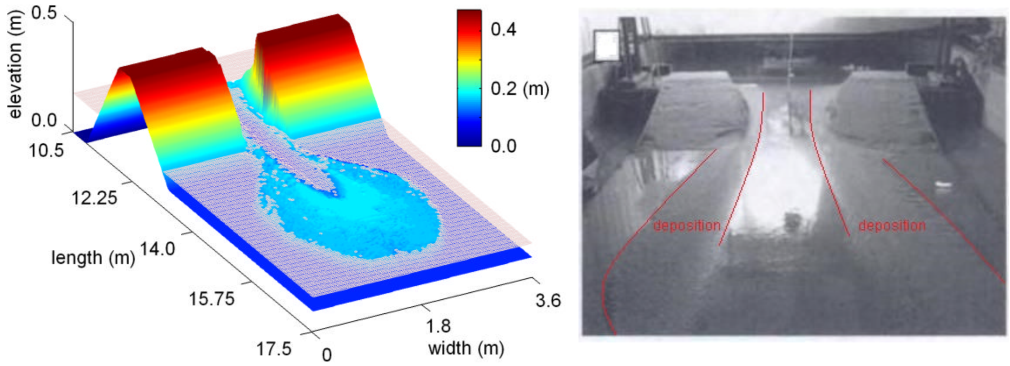

Fig.13. Simulated final dyke breach and water surface, and observed image by (Spinewine et al. 2004)

The role of bed slope avalanching

As mentioned above, the main purpose of the bed slope avalanching model in this case is to simulate the lateral erosion of the dyke. We can postulate that the dyke breach will stay constant in a horizontal direction and the erosion can only occur in vertical direction if no bed slope avalanching is implemented. Although the different critical angles and re-formation angles above and below the water are suggested by (Spinewine et al. 2004), the values of these angles are still ambiguous which directly influences the breach size and the outflow hydrograph. Also for the dyke breach process, it has been investigated by (Pickert et al. 2011) that the apparent cohesion represented by the pore-water pressure influences the stability of the breach slide slopes and thereby the whole breach process. To further investigate the effects of these angles, three runs with three different pairs of angles are implemented: run1 (82°, 34°) means the critical angles above and below the water are 82° and 34° respectively, it is similar for run2 (72°, 34°), and run3 (62°, 30°); the re-formation angles are equal to the critical angles minus 2°. For the breach cross-section profiles, comparisons for the three runs at the dyke top and the downstream slope of the dyke are given in Fig.14. It is shown that the breach width is influenced by the angles, as expected. More specifically, the smaller the critical angles, the wider the breach size, whilst the side slope of the breach is steeper for the larger critical angles. This is because the bed slope avalanching occurs at an earlier time for the smaller critical angles, and correspondingly more lateral erosion occurs. In summary, through the above analysis, we emphasise the crucial role of the critical angles in predicting the dyke breach evolution is shown.

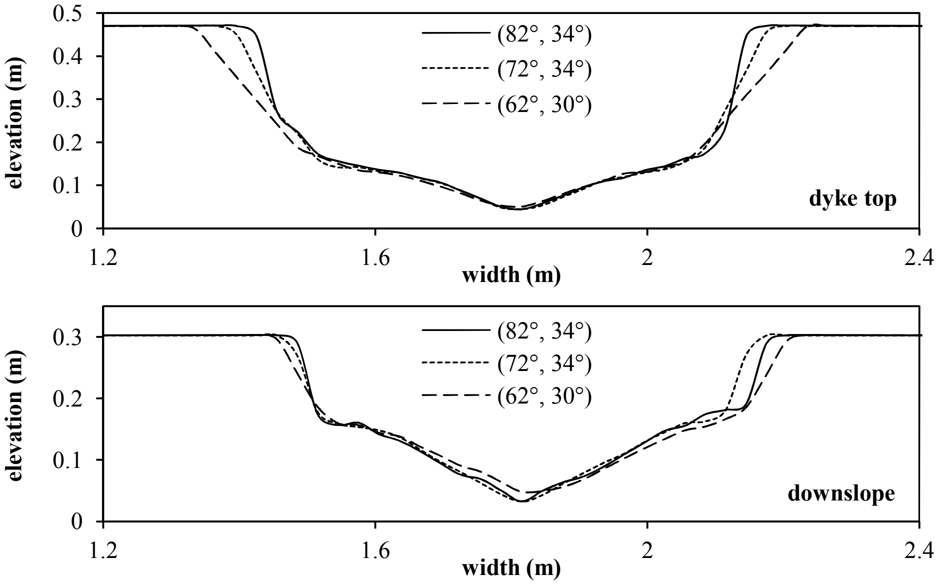

Fig.14. Predicted bed cross-sections for the three pairs of angles at the dyke top and the dyke downslope

Conclusions

Dyke breaching is a complex process and the traditional "sudden dam-break" assumption is too conservative to represent it adequately. On the other hand to estimate breach evolution and outflow discharge by empirical or simplified physical models involves many unknown factors. This paper proposes a layer-based two-dimensional hydro-morphodynamic model to predict the complex dyke breach processes. Also, a 2D bed slope avalanching model is proposed in order to calculate the lateral erosion and also maintain the stability of unstable sloped bed. The model is solved numerically with a second-order TVD-WAF/HLL which is both accurate and robust. The model is validated by several experimental benchmark tests, presenting good agreement with the measured data in terms of both hydrodynamic and morphodynamic aspects. Finally, the validated model is applied to predict a dyke breach process caused by partial flow overtopping with an initial trapezoidal shape. The complex flow-sediment process is reproduced by the model with good agreement. In short, the advantages of the 2D morphodynamic model together with the bed slope avalanching model involve:

- The key hydraulic components, the water level and the outflow hydrograph, especially peak discharge, can be predicted fairly well.

- The spatial and temporal evolutions of the dyke breach are also well reproduced, including the dyke breach shape and size, as well as the distribution of erosion and deposition in the downstream area.

The disadvantages of this approach, however, lie in the empirical parameters involved in both morphodynamic model and bed slope avalanching model. Appropriately calibrated parameters are important for the numerical results. This study is primarily focused on the small-scale flood events with flow-sediment interactions. In reality, the hydraulic and bed conditions are much more complex. Therefore, applications of the model in large-scale flood events will be investigated in subsequent research.

Acknowledgments

The first author would like to thank the China Scholarship Council (CSC) and the School of Civil Engineering at University of Leeds for their financial support for his PhD studies.

References

Armanini, A., and Di Silvio, G. (1988). "A one-dimensional model for the transport of a sediment mixture in non-equilibrium conditions." *Journal of Hydraulic Research*, 26(3), 275-292.

Cao, Z., Yue, Z., and Pender, G. (2011). "Landslide dam failure and flood hydraulics. Part II: coupled mathematical modelling." *Natural Hazards*, 59(2), 1021-1045.

Chinnarasri, C., Tingsanchali, T., Weesakul, S., and Wongwises, S. (2003). "Flow patterns and damage of dike overtopping." *International Journal of Sediment Research*, 18(4), 301-309.

Coleman, S. E., Andrews, D. P., and Webby, M. G. (2002). "Overtopping breaching of noncohesive homogeneous embankments." *Journal of Hydraulic Engineering*, 128(9), 829-838.

Faeh, R. (2007). "Numerical modeling of breach erosion of river embankments." *Journal of Hydraulic Engineering*, 133(9), 1000-1009.

Fraccarollo, L., and Capart, H. (2002). "Riemann wave description of erosional dam-break flows." *J Fluid Mech*, 461, 183-228.

Franca, M. J., and Almeida, A. B. (2004). "A computational model of rockfill dam breaching caused by overtopping (RoDaB)." *Journal of Hydraulic Research*, 42(2), 197-206.

Froehlich, D. C. (1995). "Peak outflow from breached embankment dam." *Journal of Water Resources Planning and Management*, 121(1), 90-97.

Froehlich, D. C. (2008). "Embankment Dam Breach Parameters and Their Uncertainties." *Journal of Hydraulic Engineering*, 134(12), 1708-1721.

Goutiere, L., Soares-Frazão, S., and Zech, Y. (2011). "Dam-break flow on mobile bed in abruptly widening channel: experimental data." *Journal of Hydraulic Research*, 49(3), 367-371.

Greco, M., Iervolino, M., Leopardi, A., and Vacca, A. (2012). "A two-phase model for fast geomorphic shallow flows." *International Journal of Sediment Research*, 27(4), 409-425.

Greimann, B., Lai, Y., and Huang, J. C. (2008). "Two-dimensional total sediment load model equations." *Journal of Hydraulic Engineering*, 134(8), 1142-1146.

Guan, M. F., Wright, N. G., and Sleigh, P. A. (2013). "A robust 2D shallow water model for solving flow over complex topography using homogenous flux method." *International Journal for Numerical Methods in Fluids*(10.1002/fld.3795).

Hu, C. H., and Hui, Y. J. (1996). "Bed-load transport .1. Mechanical characteristics." *Journal of Hydraulic Engineering-Asce*, 122(5), 245-254.

Li, S. C., and Duffy, C. J. (2011). "Fully coupled approach to modeling shallow water flow, sediment transport, and bed evolution in rivers." *Water Resources Research*, 47.

Macchione, F. (2008). "Model for Predicting Floods due to Earthen Dam Breaching. I: Formulation and Evaluation." *Journal of Hydraulic Engineering*, 134(12), 1688-1696.

Meyer-Peter, E., and Müller, R. (1948). "Formulas for bed load transport." *Proc., 2nd Meeting*Stockholm, Sweden, 39–64.

Morris, M. W., Hassan, M., and Vaskinn, K. A. (2007). "Breach formation: Field test and laboratory experiments."

Journal of Hydraulic Research, 45, 9-17.
Pickert, G., Weitbrecht, V., and Bieberstein, A. (2011). "Breaching of overtopped river embankments controlled by apparent cohesion." *Journal of Hydraulic Research*, 49(2), 143-156.
Pierce, M. W., Thornton, C. I., and Abt, S. R. (2010). "Predicting Peak Outflow from Breached Embankment Dams." *Journal of Hydrologic Engineering*, 15(5), 338-349.
Pontillo, M., Schmocker, L., Greco, M., and Hager, W. H. (2010). "1D numerical evaluation of dike erosion due to overtopping." *Journal of Hydraulic Research*, 48(5), 573-582.
Pugh, F. J., and Wilson, K. C. (1999). "Velocity and concentration distributions in sheet flow above plane beds." *Journal of Hydraulic Engineering*, 125(2), 117-125.
Roelvink, D., Reniers, A., van Dongeren, A., de Vries, J. v. T., McCall, R., and Lescinski, J. (2009). "Modelling storm impacts on beaches, dunes and barrier islands." *Coastal Engineering*, 56(11-12), 1133-1152.
Simpson, G., and Castelltort, S. (2006). "Coupled model of surface water flow, sediment transport and morphological evolution." *Computers & Geosciences*, 32(10), 1600-1614.
Singh, V. P. (1996). *Dam Breach Modeling Technology*, Kluwer Academic, the Netherlands.
Smart, G., and Jäggi, M. (1983). "Sediment transport on steep slopes." *Mitteilung. 64. Versuchsanstalt fu¨r Wasserbau, Hydrologie und Glaziologie, ETH Zurich, Zurich*.
Soares-Frazão, S., and Zech, Y. (2011). "HLLC scheme with novel wave-speed estimators appropriate for two-dimensional shallow-water flow on erodible bed." *International Journal for Numerical Methods in Fluids*, 66(8), 1019-1036.
Soulsby, R. (1997). *Dynamics of marine sands: a manual for practical applications*, ThomasTelford, London, UK.
Spinewine, B., Capart, H., Grelle, N., Soares-Frazão, S., and Zech, Y. "Experiments and computations of bankline retreat due to geomorphic dam-break floods." *Proc., River Flow 2002*, Balkema, Rotterdam, Netherland, 651-662.
Spinewine, B., Delobbe, A., Elslander, L., and Zech, Y. (2004). "Experimental investigation of the breach growth process in sand dikes." *Proc., Proceedings of the Second International Conference on Fluvial Hydraulics*.
Sumer, B. M., Kozakiewicz, A., Fredsoe, J., and Deigaard, R. (1996). "Velocity and concentration profiles in sheet-flow layer of movable bed." *Journal of Hydraulic Engineering*, 122(10), 549-558.
Swartenbroekx, C., Soares-Frazão, S., Staquet, R., and Zech, Y. (2010). "Two-dimensional operator for bank failures induced by water-level rise in dam-break flows." *Journal of Hydraulic Research*, 48(3), 302-314.
Toro, E. F. (1992). "Riemann problems and the WAF method for solving the two-dimensional shallow water equations." *Philosophical Transactions of the Royal Society of London Series a-Mathematical Physical and Engineering Sciences*, 338(1649), 43-68.
Toro, E. F. (2001). *Shock-Capturing Methods for Free-Surface Shallow Flows* John Wiley &Sons, LTD.
Van Emelen, S., Swartenbroekx, C., Zech, Y., and Soares-Frazão, S. "Numerical modelling of the breaching process in an earthen dike." *Proc., Fifth International Conference on Advanced COmputational Methods in ENgineering*.
van Rijn, L. C. (1984). "Sediment transport part I, bed load transport." *Journal of Hydraulic Engineering*, 110(10), 1431-1456.
Volz, C., Rousselot, P., Vetsch, D., and Faeh, R. (2012). "Numerical modelling of non-cohesive embankment breach with the dual-mesh approach." *Journal of Hydraulic Research*, 50(6), 587-598.
Wahl, T. L. (1998). "Prediction of embankment dam breach parameters—A literature review and needs assessment." *Dam Safety Rep. No. DSO-98-004*, U.S. Dept. of the Interior. Bureau of Reclamation, Denver.
Walder, J. S., and Oconnor, J. E. (1997). "Methods for predicting peak discharge of floods caused by failure of natural and constructed earthen dams." *Water Resources Research*, 33(10), 2337-2348.
Wu, W., et al. (2011). "Earthen Embankment Breaching." *Journal of Hydraulic Engineering*, 137(12), 1549-1564.
Wu, W. M. (2004). "Depth-averaged two-dimensional numerical modeling of unsteady flow and nonuniform sediment transport in open channels." *Journal of Hydraulic Engineering*, 130(10), 1013-1024.
Xia, J., Lin, B., Falconer, R. A., and Wang, G. (2010). "Modelling dam-break flows over mobile beds using a 2D coupled approach." *Advances in Water Resources*, 33(2), 171-183.
Zech, Y., Soares-Frazao, S., Spinewine, B., and Grelle, N. L. (2008). "Dam-break induced sediment movement: Experimental approaches and numerical modelling." *Journal of Hydraulic Research*, 46(2), 176-190.